

Corresponding Author:

Anthony D. Puckett
5711 Boardman Hall
Department of Mechanical Engineering
University of Maine
Orono, ME 04469
USA
Phone: +1-207-581-3071
Fax: +1-207-581-2379
anthony.puckett@umit.maine.edu

A semi-analytical model for predicting multiple propagating axially symmetric modes in cylindrical waveguides

Anthony D. Puckett, M. L. Peterson
Department of Mechanical Engineering
5711 Boardman Hall
The University of Maine
Orono, Maine 04469, USA

Abstract:

A semi-analytical model for multiple mode axially symmetric wave propagation in finite solid cylindrical waveguides is presented. The model is designed as a tool for predicting and interpreting experimental signals. The model is based on a common experimental configuration and considers the excitation, propagation and reception of the ultrasonic signal in the waveguide. The Pochhammer-Chree solution for an infinite cylinder is the basis for the model. Extensions are made to enable comparison to experimental results. Comparisons with experiment are performed in the time, frequency and joint-time frequency domain for both narrow band and broad band excitation of the piezo-electric transducer.

PACS: 43.20.Bi, 43.20.Mv, 43.35.Yb, 43.35.Zc

Keywords: cylindrical waveguide, elastic wave propagation, dispersive, multiple mode, analytical model

1. Introduction

Solid cylindrical waveguides have been used as buffer rods in a number of applications to isolate ultrasonic sensors from hostile environments [1,2,3]. In some

cases, design constraints necessitate the use of large diameter waveguides, which propagate multiple modes [3]. The propagation of multiple modes causes a signal that is compact in the time domain to have a large time signature after propagating through the waveguide, Fig. 1. As a result, if the acoustic signal is propagated through a specimen, as well as a buffer rod, measurement of phase velocity and attenuation information in the specimen is difficult. To help interpret acoustic signals of this nature a semi-analytical model for axially symmetric wave propagation in finite solid cylindrical waveguides has been developed based on the Pochhammer-Chree theory [4,5].

The Pochhammer-Chree theory is a time harmonic solution, which describes the propagation of axially symmetric waves in an infinite stress free cylindrical rod. A number of analytical models have been developed from the Pochhammer-Chree solutions to predict aspects of axially symmetric wave propagation in finite and semi-infinite cylindrical bars. Davies [6] used the phase velocities from the frequency equation and a Fourier decomposition to predict the change in shape of a trapezoidal (first mode only) excitation in a finite cylindrical bar; however, no experimental comparison was made. In a similar method Follansbee and Frantz [7] calculated a dispersion correction for signals measured in the split Hopkinson pressure bar (SHPB).

Zemanek [8] considered the stresses of the modes to determine the reflection of the first mode incident on the free end of a cylindrical bar. In addition to the fundamental mode, modes with complex wave numbers were considered in an expansion to satisfy the stress free boundary conditions. Reflection coefficients were calculated from a system of equations equal to the number of modes considered, and an end resonance was observed. Gregory and Gladwell [9] also considered the reflection of the first mode but calculated

the coefficients in the expansion using an integral formulation of least squares. The resonant frequency observed by both Zemanek and Gregory and Gladwell was very close to the experimental frequency measured by Oliver [10]. However, this was the only experimental comparison.

Peterson [11] combined the techniques of Davies and Zemanek for consideration of a finite cylindrical waveguide with a broadband excitation. Puckett and Peterson [12] refined this model by calculating the relative mode amplitudes at multiple frequencies; however, the receiving end conditions were not considered. Experimental comparisons were made with finite cylinders that considered the propagation of the first three modes.

Other methods for modeling axially symmetric wave propagation in semi-infinite cylindrical rods have also been considered. Integral transform techniques have been used to solve the boundary value problem of a semi-infinite cylindrical rod subjected to a variety of initial conditions [13-17]. For large distances the approximate solutions for wave propagation in cylindrical waveguides developed by the integral transform method are representative of experiments [15-17]. Additionally, it was shown that the solutions are independent of the end conditions at large distances. Based on analytical calculations, Jones and Norwood [18], and Kennedy and Jones [19] found the difference in peak values was insignificant at distances over 20 diameters, and the difference in average values was insignificant at distances of 5 diameters. They discussed this small difference in terms of a dynamic Saint-Venant's principle.

The integral transform solutions and the associated experiments looked solely at the response to a step function because of the simplicity of the transforms and of the interest experimentally in modeling the Split Hopkinson Pressure Bar (SHPB). However,

an analytical model is needed for acoustic signals used in ultrasonic nondestructive evaluation. These signals are arbitrary broadband signals that are not easily described by analytical functions and excite more than just the first two modes.

The techniques based on the Pochhammer-Chree theory lend themselves more easily to end conditions with arbitrary stress functions in both time and space and are the basis for the semi-analytical model described in this paper. The model has been designed to represent the experimental conditions of solid cylindrical waveguides used for nondestructive testing. The model extends the papers of Davies [6], Zemanek [8], and Gregory and Gladwell [9] to consider the excitation and propagation of an ultrasonic signal. The model also includes the receiving end conditions, which are consistent with the experimental configuration. Experimental comparisons of propagated signals demonstrate the ability of the model to capture the physics of the experimental system. Additionally, the analytic model provides more insight into the propagation of multiple mode dispersive signals in a cylindrical waveguide and improves the basic understanding of axially symmetric wave propagation in cylindrical waveguides.

2. Analytical Model for Longitudinal Wave Propagation

The semi-analytical model presented in this paper is designed as a tool for predicting and interpreting experimental signals, so the model is based on a general experimental configuration. The experimental setup associated with the waveguide consists of an ultrasonic contact transducer for exciting the ultrasonic signal in the waveguide, the waveguide, and a second ultrasonic contact transducer for receiving the signal. The excitation, propagation, and reception of the ultrasonic signal are each described by a part of the model using the Pochhammer-Chree solutions for an infinite

cylindrical bar. For a given input signal, the model predicts the measured dispersed output signal at the opposite end of a specific length waveguide.

2.1 Pochhammer-Chree theory

The Pochhammer-Chree theory describes axially symmetric wave propagation in a linearly elastic infinite isotropic homogeneous solid circular cylinder. The frequency equation is the primary result obtained from the Pochhammer-Chree theory. Using the notation of Achenbach [20] in standard cylindrical coordinates, it is expressed as:

$$\frac{2p}{a}(q^2 + k^2)J_1(pa)J_1(qa) - (q^2 - k^2)J_0(pa)J_1(qa) - 4k^2 pqJ_1(pa)J_0(qa) = 0, \quad (1)$$

where J_0 and J_1 are Bessel functions of the first kind of order zero and one respectively,

$$p^2 = \frac{\omega^2}{c_L^2} - k^2 \quad \text{and} \quad q^2 = \frac{\omega^2}{c_T^2} - k^2, \quad (2)$$

k is the wave number, ω is the circular frequency, a is the radius of the cylinder, c_L is the velocity of longitudinal waves in an unbounded medium, and c_T is the velocity of transverse waves in an unbounded medium. The wave number is equal to ω/c where c is the phase velocity.

At any frequency, an infinity of wave numbers satisfies the frequency equation. A finite number are real valued and represent propagating modes. These wave numbers are often represented graphically as dispersion curves in the form of phase velocity versus frequency, Fig. 2. There are also a finite number of imaginary wave numbers that represent nonpropagating modes. The remaining infinity of wave numbers are complex valued. The complex wave numbers are associated with the evanescent modes and appear in pairs that are the negative complex conjugate of the other. These two traveling waves form a standing wave, which decreases in amplitude spatially as $z \rightarrow +\infty$ and does

not transport energy. The stresses and displacements of the evanescent modes provide the remaining infinity of stress and displacement functions necessary to satisfy an arbitrary boundary condition on the end of a semi-infinite or finite cylindrical bar.

The stresses and displacements in cylindrical coordinates, associated with mode j , referred to later as stress functions and displacement functions, are defined as:

$$u^{(j)} = -[pJ_0(pr) + iC^{(j)}k^{(j)}J_1(qr)], \quad (3)$$

$$w^{(j)} = ik^{(j)}J_0(pr) + C^{(j)}qJ_1(qr), \quad (4)$$

$$\sigma_{zz}^{(j)} = -J_0(pr)[\lambda(p^2 + (k^{(j)})^2) + 2\mu(k^{(j)})^2] + 2\mu C^{(j)}iqk^{(j)}J_0(qr), \quad (5)$$

$$\text{and } \sigma_{rz}^{(j)} = -\mu[2ik^{(j)}pJ_1(pr) + C^{(j)}(q^2 - (k^{(j)})^2)J_1(qr)], \quad (6)$$

$$\text{where } C^{(j)} = \frac{-2ik^{(j)}pJ_1(pa)}{(q^2 - (k^{(j)})^2)J_1(qa)}, \quad (7)$$

λ and μ are the Lamé constants, r is the radial coordinate, z is the axial coordinate, $\sigma_{zz}^{(j)}$ is the normal stress, $\sigma_{rz}^{(j)}$ is the shear stress, $w^{(j)}$ is the normal displacement, $u^{(j)}$ is the radial displacement, and $k^{(j)}$ is the wave number [21]. (The factor $\exp(ik^{(j)}z - i\omega t)$ has been suppressed.) The stresses and displacements are a function of both radius and frequency, Fig. 3.

2.2 Parts of the Model

The frequency dependence of the Pochhammer-Chree solutions compels that the operations of the analytical model be performed in the frequency domain. All operations are conducted in the frequency domain unless noted otherwise. The time representation of the dispersed signal, $x_d(t)$, that has propagated through the waveguide can be

represented as the inverse Fourier transform of the frequency spectrum of the dispersed signal, $X_D(\omega)$, Eq. (8) [11].

$$x_d(t) = \int_{-\infty}^{\infty} X_D(\omega) e^{i\omega t} d\omega \quad (8)$$

The dispersed signal can be represented by the input reference signal, $X_R(\omega)$, multiplied by a dispersion function, $F_D(\omega)$, Eq. (9).

$$X_D(\omega) = X_R(\omega) F_D(\omega) \quad (9)$$

The dispersion function is a transfer function that represents the dispersion in the waveguide. The dispersion function contains the effects of all of the modes and is equal to the sum of the transfer functions of the modes.

The transfer function of each mode is determined from the three parts of the experimental setup: the transmission from the exciting transducer to the waveguide, the propagation through the waveguide, and the transmission from the waveguide to the receiving transducer. The phase information of the transfer function is dictated by the propagation of the mode through the waveguide, and the amplitude is provided by the boundary conditions on both ends of the cylindrical rod.

2.3 Excitation

The excitation on the end of the waveguide determines the relative amplitudes of the modes. An ultrasonic contact transducer excites the ultrasonic signal into the waveguide, so the characteristics of the transducer determine the boundary conditions on the end of the cylindrical bar. The transducer exhibits a pressure, $P(r)$, on the end of the cylinder, which specifies the normal stress boundary condition. This boundary condition

is a function of radius and can be represented by an expansion over the normal stress function, $\sigma_{zz}^{(j)}$.

$$P(r) = \sum_j A^{(j)} \sigma_{zz}^{(j)}(r), \quad (10)$$

where $A^{(j)}$ and $\sigma_{zz}^{(j)}$ are associated with the wave number $k^{(j)}$ of mode j . (Previous authors have made compelling arguments that the stress functions of the modes form a complete set [9,22].) The coefficients in the expansion, $A^{(j)}$, are equal to the amplitudes of the modes.

Either the shear stress or the radial displacement specifies the second boundary condition on the end of the bar. A viscous fluid coupling is used between the transducer and the bar, so the shear stress, $\sigma_{rz}^{(j)}$, is assumed to be zero. Therefore, the amplitudes of the modes must also satisfy an expansion over the radial shear stress functions,

$$0 = \sum_j A^{(j)} \sigma_{rz}^{(j)}(r). \quad (11)$$

These two expansions are usually written as a single expansion [for example 8,9].

There are a number of approaches to calculating the coefficients, $A^{(j)}$, in the expansion. The first choice is to use the orthogonality relations of the functions, if available. These relations have been developed by Fama [22] for the elastostatic case, and Fraser [21] demonstrated that the relations also applied to the elastodynamic case.

The orthogonality relation for a cylinder with a stress free lateral surface is expressed as:

$$\int_0^a (w^{(j)} \sigma_{zz}^{(l)} - \sigma_{rz}^{(j)} u^{(l)}) r dr = 0 \quad j \neq l \quad [21, \text{Eq. (17)}]. \quad (12)$$

For the case of pure stress end conditions this relation does not provide a direct solution for the coefficients [22, Eq. (10)]. However, Fama shows there is a unique solution for the coefficients in the pure end condition problem.

Zemanek [8] used a simple method to solve for the coefficients, a system of equations. The number of equations was dictated by the number of modes of interest. The same number of points were considered along the radius, and for each point an equation was generated from either, Eq. (10) or Eq. (11). This technique works well when a large number of modes are being considered. However, at the lowest frequencies there is only one propagating mode, so evanescent modes must be considered for better accuracy.

Gregory and Gladwell [9] used an integral formulation of least squares to evaluate the coefficients. In the present model the expansion is evaluated at discrete points using a least squares technique to solve the coefficients. This technique is more accurate than the system-of-equations and allows more points to be evaluated since the system of equations is overdetermined. Additionally, the least squares relation can be derived directly from the expansion, Eq. (10), by rewriting the equation to include a residual error, e :

$$P(r) = \sum_j A^{(j)} \sigma_{zz}^{(j)}(r) + e, \text{ or } \{P\} = [\sigma]\{A\} + \{e\}. \quad (13)$$

When the sum of the squares of the residuals is minimized the coefficients can be expressed in matrix notation as:

$$\{A\} = \left[[\sigma]^T [\sigma] \right]^{-1} [\sigma]^T \{P\}. \quad (14)$$

In the limit as the residual error approaches zero the coefficients are the exact solution.

This equation provides the amplitudes of the modes.

The main issue with the least squares method and any collocation method is the number of modes to consider in the expansion. For any number of modes in the expansion the accuracy of the coefficients can be found by summing the series, Eq. (10) and Eq. (11), and comparing the value to the applied pressure excitation, $P(r)$, at points along the radius. An increase in the number of modes considered in the expansion will increase the accuracy even if only slightly. At the lowest frequencies where only a small number of modes propagate, evanescent modes must be considered for an accurate value of the amplitudes to be calculated. At higher frequencies only the propagating modes may be sufficient to accurately calculate the coefficients in the expansion.

2.4 Propagation

Each of the propagating modes has a different phase velocity, which varies with frequency. The phase velocity provides a phase shift in the transfer function of the mode. The length of the waveguide divided by the phase velocity is the time for a point of constant phase in a continuous harmonic wave to travel the length of the waveguide. This time delay is a phase shift in the frequency domain. The phase shift is represented as:

$$\Phi^{(j)}(\omega) = e^{(i\omega L/c^{(j)})}, \quad (15)$$

where $c^{(j)}$ is the phase velocity of mode j at frequency ω . This technique has also been used by Kohl, Datta and Shah [23] in semi-infinite hollow cylinders and by Peterson [11] whose model is refined in this paper. The evanescent modes are not considered in the propagation because the modes have at least 40 dB of attenuation at a distance of 20 diameters, and at 5 diameters the effects are negligible.

2.5 Reception

The transmission from the waveguide to the receiving transducer adds another amplitude factor to the transfer function of each mode. Ideally this interface is modeled as a reflection problem, with the stresses and displacements continuous at the interface, to determine the reflected and transmitted energy. Experimentally, a viscous fluid coupling is used between the waveguide and the transducer, so no shear stress is transmitted. However, the normal stress excites the normal modes of the piezo-electric transducer. The contact transducer is modeled as an immersion transducer, which has a response that is proportional to the average normal pressure over the face of the transducer [24]. The average pressure exhibited on the transducer by a single mode is calculated by integrating the normal stress of the mode, $\sigma_{zz}^{(j)}$, over the area of the bar and dividing by the area. The average pressure is an additional amplitude factor in the transfer function of a mode, and it is only calculated for the propagating modes.

2.6 Final Model

The combination of the three parts of the model gives the final form of the dispersion function, which is the sum of the transfer functions of the propagating modes, Eq. (16).

$$F_D(\omega) = \sum_j A^{(j)}(\omega) \cdot \Phi^{(j)}(\omega) \cdot \frac{2}{a^2} \int_0^a r \sigma_{zz}^{(j)}(\omega, r) dr. \quad (16)$$

The transfer function of each propagating mode contains a relative amplitude term from the excitation, $A^{(j)}(\omega)$, a phase shift term from the propagation, $\Phi^{(j)}(\omega)$, and an additional amplitude term representing the average normal stress. It should be noted that if the phase velocity was the same for all of the modes and did not change with frequency, then

the phase shift, $\Phi^{(j)}(\omega)$, would be the same for all of the modes at each frequency. This would allow the phase shift to move outside the summation, and therefore the dispersion function would reduce to a term consisting of the phase shift times the average pressure of the excitation. This is the case for a thin bar where only the first mode propagates and the phase velocity is equal to the bar velocity, $c_b = \sqrt{E/\rho}$.

2.7 Discretization

The complexity of the Pochhammer-Chree theory and the arbitrary nature of the ultrasonic signals that are considered dictate that the calculations be best made numerically and thus at discrete frequency intervals. A discrete Fourier transform (DFT) pair, Eqs. (17) and (18), is used to transform between the time domain and the frequency domain. A lowercase letter is used to denote the time domain and an upper case letter is used to denote the frequency domain.

$$F\{x(n)\} \Rightarrow X[m] = \sum_{n=0}^{N-1} x[n]e^{-inm(2\pi/N)} \quad m = 0,1,\dots,N-1. \quad (17)$$

$$F^{-1}\{X(m)\} \Rightarrow x[n] = \frac{1}{N} \sum_{m=0}^{N-1} X[m]e^{inm(2\pi/N)} \quad n = 0,1,\dots,N-1, \quad (18)$$

where the index n corresponds to time, the index m corresponds to frequency, and N is the number of points in the DFT.

The substitution of the dispersion function into Eq. (9) and Eq. (9) into the discrete version of Eq. (8) yields the final form of the model,

$$x_d(n) = \frac{1}{N} \sum_{m=0}^{N-1} \left[\sum_j A^{(j)}(m) \cdot \Phi^{(j)}(m) \cdot \frac{2}{a^2} \int_0^a r \sigma_{zz}^{(j)}(m,r) dr \cdot X_R(m) \right] e^{inm(2\pi/N)}. \quad (19)$$

The phase shift is represented discretely as:

$$\Phi^{(j)}(m) = e^{(-im[L/c^{(j)}(m)/\Delta t](2\pi/N)}, \quad (20)$$

where $c^{(j)}(m)$ is the phase velocity of mode j at frequency m , and Δt is the time step. The operations within the square brackets of Eq.(19) are calculated at each frequency.

2.8 Discussion

This model calculates the change of a signal after propagating through a finite length cylindrical bar. The lengths of interest, greater than 5 diameters, are sufficiently in the far field, so only the propagating modes need to be considered for the propagation and reception portions of the model. However, at the lowest frequencies only a small number of modes propagate. The consideration of only these modes may provide insufficiently accurate results in the expansion to determine the amplitudes of the modes. To ensure sufficient accuracy, evanescent modes should also be considered in the expansion. Thus, an area of concern with the model is the number of modes to consider in the calculations.

The least squares method of solving the coefficients in the expansion is quite robust, so the results do not typically change much with an increase in the number of modes. Transfer functions of the first four modes were calculated using various numbers of modes in the expansion, including just the real modes and up to nine modes. It was found that the difference in the calculated transfer functions of the individual modes was typically less than two percent of the maximum value except for the range of frequencies before the second mode cutoff frequency where the difference was larger. However, it was found that at high frequencies with a large number of propagating modes, considering nine modes in the expansion provided good results.

Similar results were also observed when only the normal stress was considered in the expansion. This is also a result of considering bars with lengths that are in the far

field. From an experimental standpoint the negligible effects of the second boundary condition can be thought of in terms of a dynamic Saint-Venant's principle.

The evaluation of the expansion at a discrete number of points along the radius produces some obvious erroneous calculations at some frequencies. It was often found that just above a mode's cutoff frequency the amplitude of the mode would often spike along with one of the lower modes. The nature of the mode shapes required large offsetting amplitudes to satisfy the boundary conditions. However, it was found that if the number of modes considered was limited, the errors disappeared. The algorithm that provided the best results considered a fixed number of modes on either side of the mode with the largest average normal stress.

A number of additional steps were used to simplify the model and minimize numerical problems. The stress functions of the modes are complex valued at any given radius, so the coefficients in the expansion are complex as well. However, the phase shift of each stress function can be calculated to eliminate the imaginary part of the stress function. The real form of the stress functions simplifies both the matrix operations and the integration and produces a real coefficient.

The amplitudes of the stress functions change with frequency; therefore, it is prudent to also normalize the real form of the stress functions to help prevent the matrix from becoming singular. This also ensures that the stresses are the same order of magnitude as the applied excitation pressure. It is necessary that the same form of the stress functions be used in the expansion and the integration, so that there are no erroneous phase or amplitude terms added to the transfer functions.

3. Experimental comparison of analytical model

A number of experiments in a through-transmission configuration were performed for comparison to the analytical model. The signals and the size of the waveguides used in the experiments are representative of ultrasonic NDE experiments [e.g. 2,3]. The application of the analytical model is discussed in the description of the experiments.

The experiments used two 38 mm diameter, 1 MHz broadband, longitudinal contact transducers [Panametrics, model V194, Waltham, MA] to excite and receive the ultrasonic signals. The transducers had a bandwidth, corresponding to a 6 dB drop in the peak amplitude of the spectrum, of 0.4 MHz to 1.1 MHz. The pressure distribution over the area of the transducers was nearly uniform [25]. Therefore, the pressure distribution, $P(r)$, used in the analytical model was prescribed as having a value of unity at all radii and for all frequencies.

Signals were provided by two different sources depending on the experiment. For one of the experiments a pulser/reciever [Panametrics, 5072PR, Waltham, MA] was used to generate a pulse and amplify the received signal. For the other experiments an arbitrary waveform generator [Agilent 33250A, Palo Alto, CA] was used to generate more complex signals to drive the transducer. With this configuration a radio frequency power amplifier [ENI A-300, Rochester, NY] with a gain of 55 dB was used to amplify the signal to the transducer, and the signal generated by the receiving transducer was amplified by an ultrasonic pre-amplifier [Panametrics model 5660C, Waltham, MA] with a gain of 40 dB. For both setups the amplified signal was averaged to remove noise and recorded by a digital storage oscilloscope [Tektronix TDS 520A, Wilsonville, OR].

Waveguides of 25 mm diameter fused quartz cylindrical rods were used. Lengths of 0.2 m ($34 \lambda_L$), 0.25 m ($42 \lambda_L$) and 0.5 m ($85 \lambda_L$) were considered where λ_L is the

wavelength of a longitudinal wave in an infinite medium at 1 MHz. An amorphous material was chosen for the waveguide because linear elastic and homogeneous assumptions are well satisfied. The properties of the fused quartz rods used in the experiments are a Young's modulus, E , of 72 GPa, a density, ρ , of 2200 kg/m³, and a Poisson's ratio, ν , of 0.162. A coupling fluid [Sonotech, Inc. UT-30, State College, PA] was used between the transducers and the waveguide to improve the transmission of the ultrasonic signal.

3.1 Narrow Band

The first experiments considered the 0.25 m long, 25 mm diameter, fused quartz waveguide excited by a Gaussian modulated sine wave. Two different frequencies of the sine wave are shown that compare the results of the experiments to the analytical model. The first frequency, at 1 MHz, coincides with the maximum group velocity of the 6th propagating mode. The other frequency, at 1107 kHz, was chosen so that the group velocities of all of the modes were well below the velocity of a longitudinal wave in an infinite medium, in this case, the dip in the group velocity curves following the maximum group velocity of the 6th mode. Fig. 4 displays the group velocity curves for the 25 mm quartz waveguide with the vertical dashed lines defining the two frequencies. For each frequency the signal was propagated through the waveguide experimentally and calculated using the model

For the model, the discrete Fourier transform (DFT) of the Gaussian was used as X_R , the reference signal. Dispersion curves (in a wave numbers vs. frequency domain) were calculated for the propagating modes at the appropriate frequencies prior to running the model. At each frequency step the phase velocities and the normal stress functions

were used to calculate the complex value of the dispersion function, $F_D(\omega)$. To evaluate the coefficients, $A^{(j)}$, in the expansion, 100 points along the radius were considered. Therefore, in Eq. (14) the pressure, $\{P\}$, is a 100×1 column vector, all entries have a value of unity for the constant pressure distribution. The stress, $[\sigma]$, is a $100 \times j$ matrix where j represents the number of modes being considered. Each column of the matrix contains the values of the normal stress (Eq. 5) along the radius for one of the modes being considered. For the two Gaussian signals, all of the energy is in the higher propagating modes, so only the propagating modes were considered in the expansion. For the phase shift, $\Phi^{(j)}(\omega)$, the length of the rod (0.25m) and the phase velocity are used. The phase velocity is calculated from the wave number by $c^{(j)} = \omega/k^{(j)}$. Finally, the average normal stress over the end of the waveguide is calculated for each mode. The coefficient for each mode is multiplied by its phase shift and average pressure. This product is summed with the products calculated for the other modes to produce the value of the dispersion function for that frequency. These calculations are repeated at each frequency step. The inverse DFT of the dispersion function multiplied by the spectrum of the excitation signal is the calculated dispersed signal. This calculated dispersed signal is compared to the measured dispersed signal.

Fig. 5 compares the input Gaussian signal (top) to the experimental signal (middle) and the analytical signal (bottom) for the 1 MHz frequency. There is good agreement between the analytical signal and the experimental signal, and both signals exhibit very little dispersion. This is not the case for the second frequency. Dispersion is much more apparent in the comparison of the signals from the 1107 kHz Gaussian

excitation, Fig. 6. Despite the dispersion, the analytical and experimental signals are still very similar.

3.2 Broadband

The ability of the model was also considered with a broadband excitation. As an example, a pulse excitation of the transducers was used with the 0.5m long 25 mm diameter quartz waveguide. There are 13 modes that have cutoff frequencies below the upper 6-dB limit of the frequency spectrum of the pulse. The same procedure was used for the analytical model, and again only the propagating modes were considered in the expansion because the frequency spectrum of the signal contains very little energy in the first modes.

Fig. 7 compares the experimental and analytical signals through the 0.5 m long waveguide. For this excitation trailing pulses are observed, which are consistent with plane wave theory [26]. The general shape between the analytical and experimental signals is very similar, and the arrival times and the amplitudes of the pulses are in good agreement. The analytical model appears to capture nearly all of the physics of the wave propagation in the cylindrical waveguide in this experimental configuration.

A comparison in the frequency domain indicates similar results. The top graph in Fig. 8 is the magnitude of the dispersion function for the 0.2 m long 25 mm diameter quartz bar calculated by the model. There are observed dips in the dispersion function, but these characteristics are also observed experimentally. The lower graph in Fig. 8 is the magnitude of the frequency spectrum of an experimental signal measured in the quartz bar. For comparison, the magnitude of the frequency spectrum of the excitation signal is also shown, middle graph Fig. 8. Similar dips appear in the frequency spectrum

of the measured experimental signal and at the same locations as the dispersion function. These dips are a result of the insensitivity of the receiving transducer to radial variations in the normal stress. It is advantageous to consider the transfer functions of the modes to explain the occurrence of the dips

The transfer functions of the 1st, 6th, and 7th modes for the 0.5 m long waveguide are plotted in the lower graph of Fig. 9 (other modes are not shown for clarity). The upper graph of Fig. 9 shows the dispersion function for this waveguide. A comparison of the two graphs indicates that the large dips in the transfer function of the waveguide appear at frequencies where the magnitudes of the transfer functions of two neighboring modes are equal. The phase velocities of the two modes at these frequencies are different. For certain length bars the modes will be entirely out of phase at the receiving end of the bar, and the magnitudes will cancel each other. Similar effects are observed at other frequencies though not as pronounced. In all cases it is a result of the interaction of the modes. The energy is present; however, the superposition of the normal stress of the modes over the radius is such that the energy is not measured because the response of the transducer is proportional to the average normal stress. It must be stressed though that the model is intended to represent the experiment not mathematical modeling. Similar models that do not include receiving end conditions have been used in theoretical studies and have shown to satisfy energy criteria [9,27].

The transfer functions of the modes also illustrate that each mode is dominant over a small frequency range. This is consistent with the observations of Zemanek [28] who found that the stress function of a mode is entirely in phase when the group velocity is close to the longitudinal wave speed. The experiments and the model used a uniform

excitation across the radius of the cylindrical bar, which most excites the modes whose normal stress functions are in phase. The averaging over the area of the normal stress of the receiving transducer further emphasizes the modes that are in phase.

For broadband signals an additional domain for further comparison of the calculated dispersed signal with experimentally measured dispersed signal is the time-frequency domain. One standard tool to analyze ultrasonic signals is the short-time Fourier transform (STFT) [e.g. 29]. The energy density spectrum of the STFT, called a spectrogram, can be used to visualize the results of a STFT. Spectrograms of a Gaussian signal propagated through a 1.22 m long 10 mm diameter fused quartz cylinder are compared. The spectrograms of the measured experimental signal and the analytical signal appear in Fig. 10 and Fig. 11 respectively, with the theoretical curves in black. These curves are the calculated arrival times of the modes based on the group velocity curves. In both spectrograms the individual modes are apparent and follow the analytical curves. Additionally, the same modes appear in both spectrograms.

4. Conclusions

An analytical model for wave propagation in cylindrical waveguides has been presented. The model uses the solutions of the Pochhammer-Chree theory to calculate the dispersed signal measured at the end of the waveguide. The analytic model is designed around a general experimental configuration and considers three parts, the excitation of the ultrasonic signal into the waveguide, the propagation of the signal in the waveguide and the reception of the ultrasonic signal. The relative amplitudes of the modes are determined at each frequency by the boundary conditions on the end of the

waveguide. The phase shift is calculated from the phase velocity and the length of the waveguide.

The ability of the model was demonstrated in a number of experiments. In the time domain the dispersed signals calculated by the analytical model were found to be similar to the experimentally measured dispersed signals for both narrow band and broadband excitation signals. Comparison in the frequency domain and the time-frequency domain showed similarly good results. It was shown that the model captures the general physics of multiple mode wave propagation in cylindrical waveguides in this experimental configuration.

The ability of the analytical model to capture the physics of the wave propagation allows the model to be used to explore the behavior of wave propagation in the waveguide. The transfer function of the waveguide has already indicated that different modes dominate over certain frequency ranges. This is consistent with the observation of Zemanek [12] that the stress functions of a mode are entirely in phase when the group velocity is close to the longitudinal wave speed.

This model assumes linear elastic homogeneous isotropic materials. If these criteria are not satisfied, calculated signals may not agree well with experiments. A possible extension of this work could consider the use of modes sensitive to anisotropy to characterize the radial material properties of the waveguide.

Acknowledgements

This research is sponsored by the Ballistic Missile Defense Organization through Dr. Y. D. S. Rajapakse of the Office of Naval Research. Additional support was

provided by the National Science Foundation (NSF) GK-12 “Sensors!” grant at the University of Maine. The assistance of S. Vel on the least squares method expansion is also appreciated.

References

- [1] C.K. Jen, Ph. de Heering, P. Sutcliffe, J.F. Bussiere, Ultrasonic monitoring of the molten zone of single-crystal germanium, *Mater. Eval.* 49 (1991) 701-705.
- [2] C.-K. Jen, B. Cao, K.T. Nguyen, C.A. Loong, J.-G. Legoux, On-line ultrasonic monitoring of a die-casting process using buffer rods, *Ultrasonics* 35 (1997) 335-344.
- [3] M.L. Peterson, A signal processing technique for measurement of multi-mode waveguide signals: an application to monitoring of reaction bonding in silicon nitride, *Res. Nondestr. Eval.* 5 (1994) 239-256.
- [4] L. Pochhammer, Über die Fortpflanzungsgeschwindigkeiten kleiner Schwingungen in einem unbegrenzten isotropen Kreiscylinder, *J. Reine Angew. Math.* 81 (1876) 324-336.
- [5] C. Chree, The equations of an isotropic elastic solid in polar and cylindrical coordinates, their solution and application, *Trans. Cambridge Phil. Soc.* 14 (1889) 250-369.
- [6] R.M. Davies, A critical study of the Hopkinson Pressure Bar, *Phil. Trans. Royal Soc.* A240 (1948) 375-457.
- [7] P.S. Follansbee and C. Frantz, Wave propagation in the split Hopkinson pressure bar, *J. Eng. Mat. Tech.* 105 (1983) 61-66.
- [8] J. Zemanek, An experimental and theoretical investigation of elastic wave propagation in a cylinder, Ph. D. Diss., University of California, Los Angeles, (1962).
- [9] R.D. Gregory, I. Gladwell, Axisymmetric waves in a semi-infinite elastic rod, *Q. Jl Mech. appl. Math* 42 (1989) 327-337.
- [10] J. Oliver, Elastic wave dispersion in a cylindrical rod by a wide-band short-duration pulse technique, *J. Acoust. Soc. Am.* 29 (1957) 189-194.
- [11] M.L. Peterson, Prediction of longitudinal disturbances in a multi-mode cylindrical waveguide, *Exp. Mech.* 39 (1999) 36-42.
- [12] A.D. Puckett, M.L. Peterson, Fidelity of an analytical time reversal mirror, in *Review of Progress of Quantitative Nondestructive Evaluation Vol. 21*, edited by D.O. Thompson and D.E. Chimenti, American Institute of Physics, New York (2002) 945-952.
- [13] R. Skalak, Longitudinal impact of a semi-infinite circular elastic bar, *J. Appl. Mech.* 24 (1957) 59-64.
- [14] F. Vales, S. Moravka, R. Brepta, J. Cerv, Wave propagation in a thick cylindrical bar due to longitudinal impact, *JSME Int. J.* 39A (1996) 60-70.
- [15] R. Folk, G. Fox, C.A. Shook, C.W. Curtis, Elastic strain produced by sudden application of pressure to one end of a cylindrical bar. I. Theory, *J. Acoust. Soc. Am.* 30 (1958) 552-558.
- [16] G. Fox, C. W. Curtis, Elastic strain produced by sudden application of pressure to one end of a cylindrical bar. II. Experimental observations, *J. Acoust. Soc. Am.* 30 (1958) 559-563.
- [17] I. S. Goldberg, R.T. Folk, Solutions to time-dependent pure-end condition problems of elasticity: pressure-step wave propagation and end-resonance effects, *SIAM J. of Appl. Math.* 53 (1993) 1264-1292.

- [18] O.E. Jones, F.R. Norwood, Axially symmetric cross-sectional strain and stress distributions in suddenly loaded cylindrical elastic bars, *J. Appl. Mech.* 34 (1967) 718-724.
- [19] L.W. Kennedy, O.E. Jones, Longitudinal wave propagation in a circular bar loaded suddenly by a radially distributed end stress, *J. Appl. Mech.* 36 (1969), 470-478.
- [20] J.D. Achenbach, *Wave Propagation in Elastic Solids*, North Holland, Amsterdam, 1999.
- [21] W.B. Fraser, An orthogonality relation for the modes of wave propagation in an elastic circular cylinder, *J. Sound Vibrat.* 43 (1975) 568-571.
- [22] M.E. Fama, Radial eigenfunctions for the elastic circular cylinder, *Q. Jl. Mech. appl. Math.* 25 (1972) 479-495.
- [23] T. Kohl, S.K. Datta, A.H. Shah, Axially symmetric pulse propagation in semi-infinite hollow cylinders, *AIAA J.* 30 (1992) 1617-1624.
- [24] L.W. Schmerr, *Fundamentals of Ultrasonic Nondestructive Evaluation*, Plenum Press, New York, 1998.
- [25] A.D. Puckett, M.L. Peterson, Technique for determining the pressure distribution on the face of a contact ultrasonic transducer, *Exp. Tech.* 27(4) (2003) 37-39.
- [26] M. Redwood, *Mechanical Waveguides*, Pergamon Press, New York, 1960.
- [27] N. Rattanawangcharoen, A.H. Shah, S.K. Datta, Reflection of waves at the free edge of a laminated circular cylinder, *J. Appl. Mech.* 61 (1994) 323-329.
- [28] J. Zemanek, An experimental and theoretical investigation of elastic wave propagation in a cylinder, Ph.D. Diss., University of California, Los Angeles, (1962).
- [29] M. Niethammer, L.J. Jacobs, Time-frequency representations of Lamb waves, *J. Acoust. Soc. Am.* 109 (2001) 1841-1847.

Figures:

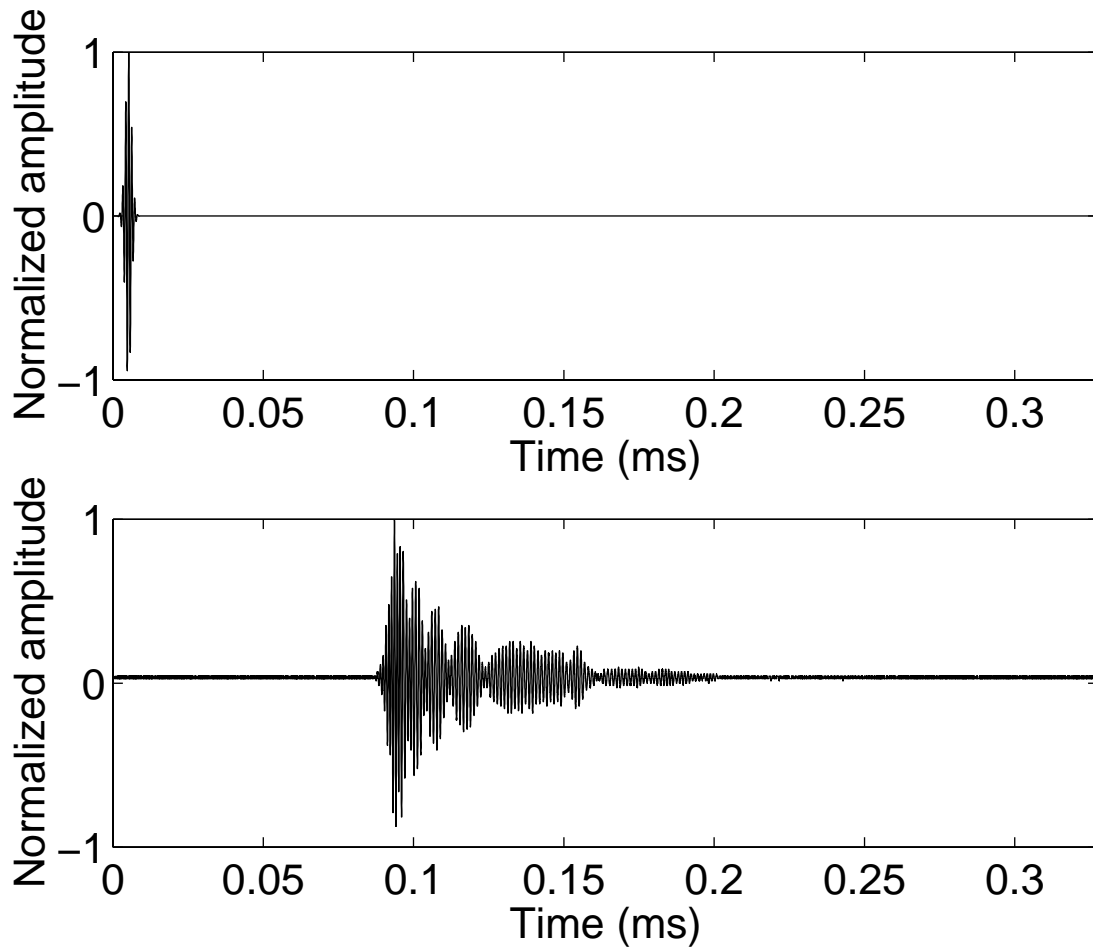


Fig. 1. Illustration of dispersion in a cylindrical waveguide. The top graph is the original signal with compact time domain. The bottom graph is the original signal after propagating through a cylindrical waveguide.

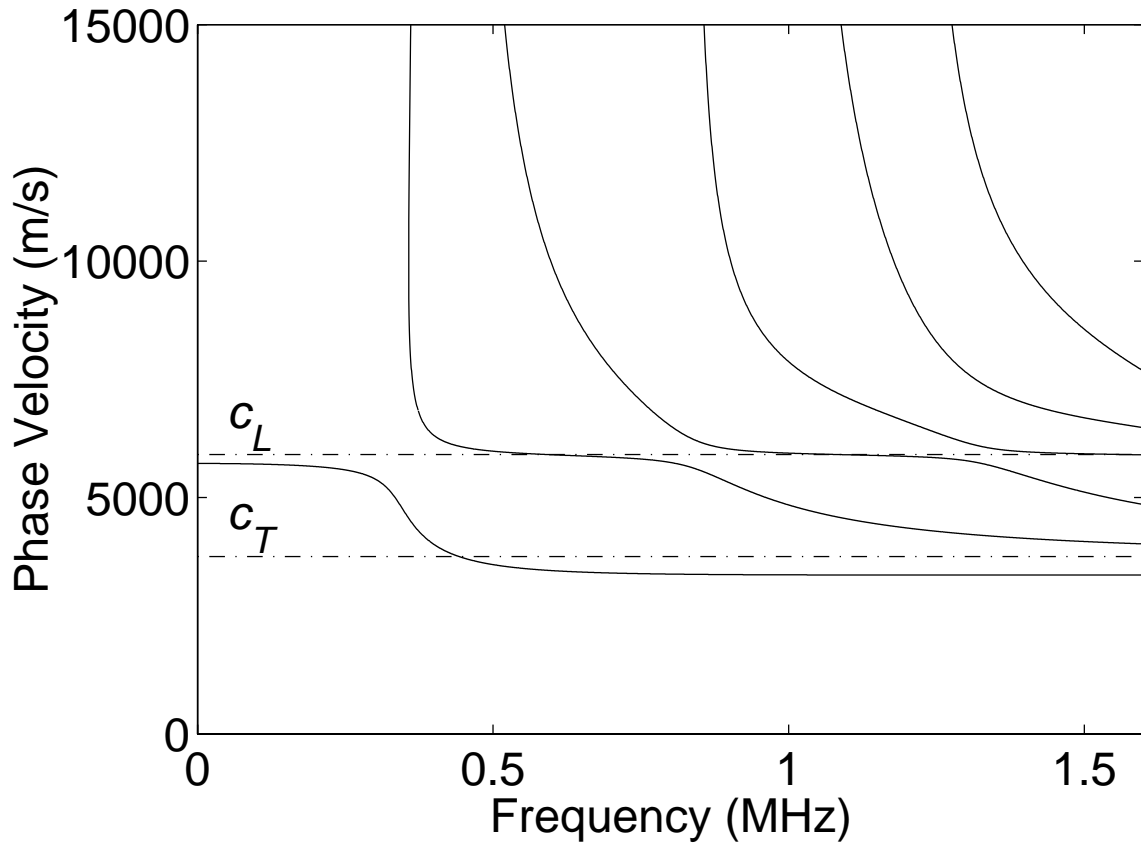


Fig. 2. Phase velocity curves for a 10 mm diameter fused quartz waveguide.

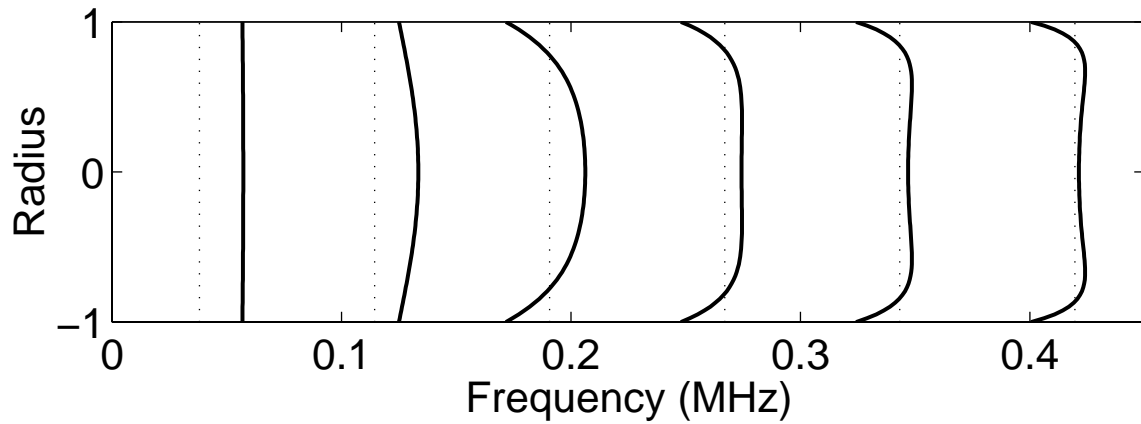


Fig. 3. Illustration of frequency dependence of normal stress. The normalized normal stress is plotted at different frequencies. The vertical dashed lines indicate zero stress and the frequency at which the stress is considered.

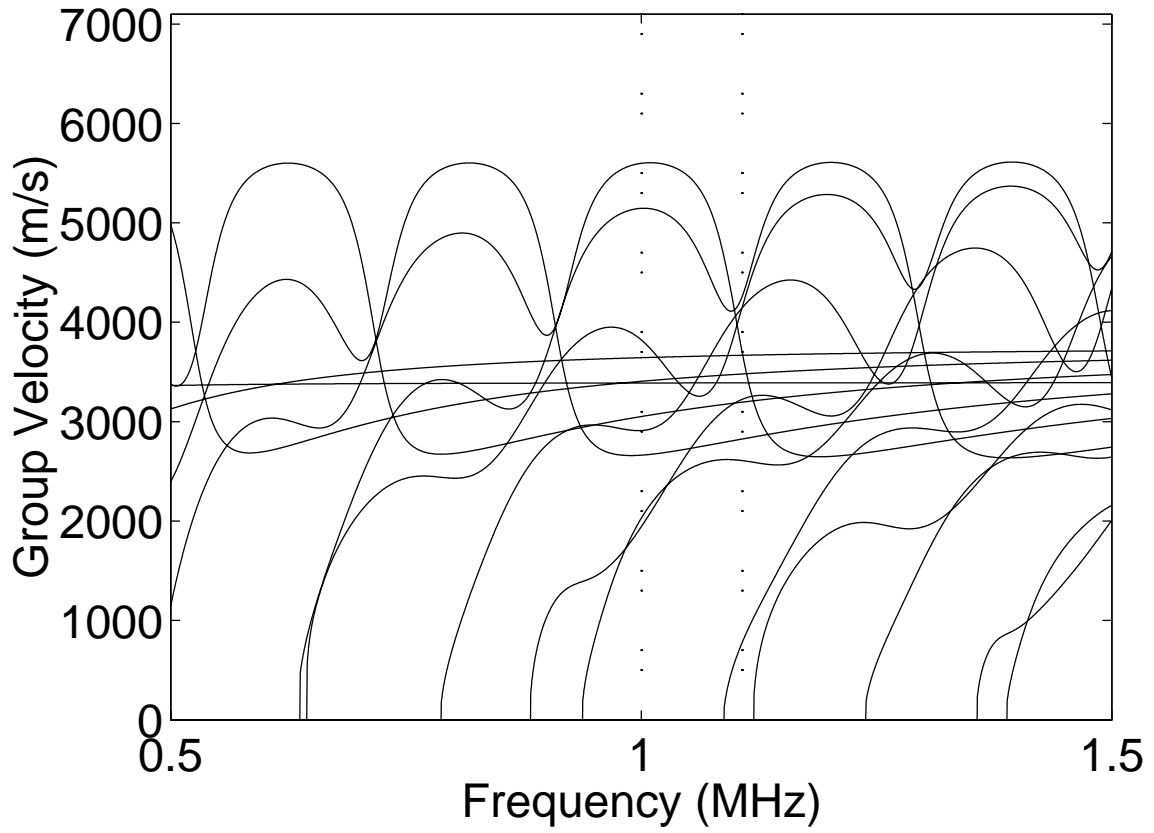


Fig. 4. Group velocity curves of a 25 mm diameter fused quartz bar. The vertical dotted lines indicate the frequencies used in the Gaussian excitations.

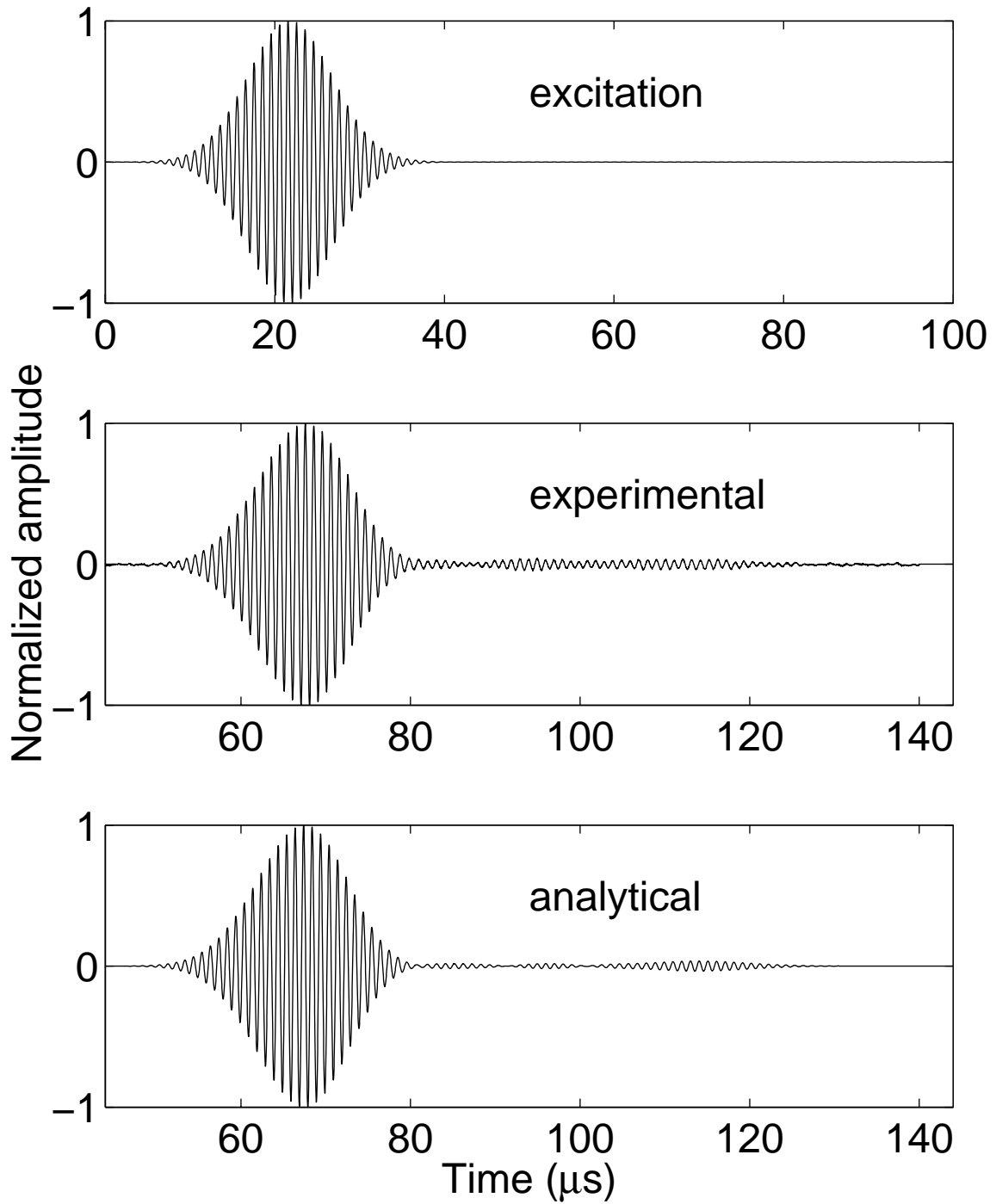


Fig. 5. 1 MHz Gaussian excitation of a 0.25m long 25 mm diameter fused quartz waveguide. The excitation signal (top) is compared to the experimental received signal (middle) and the analytical signal (bottom).

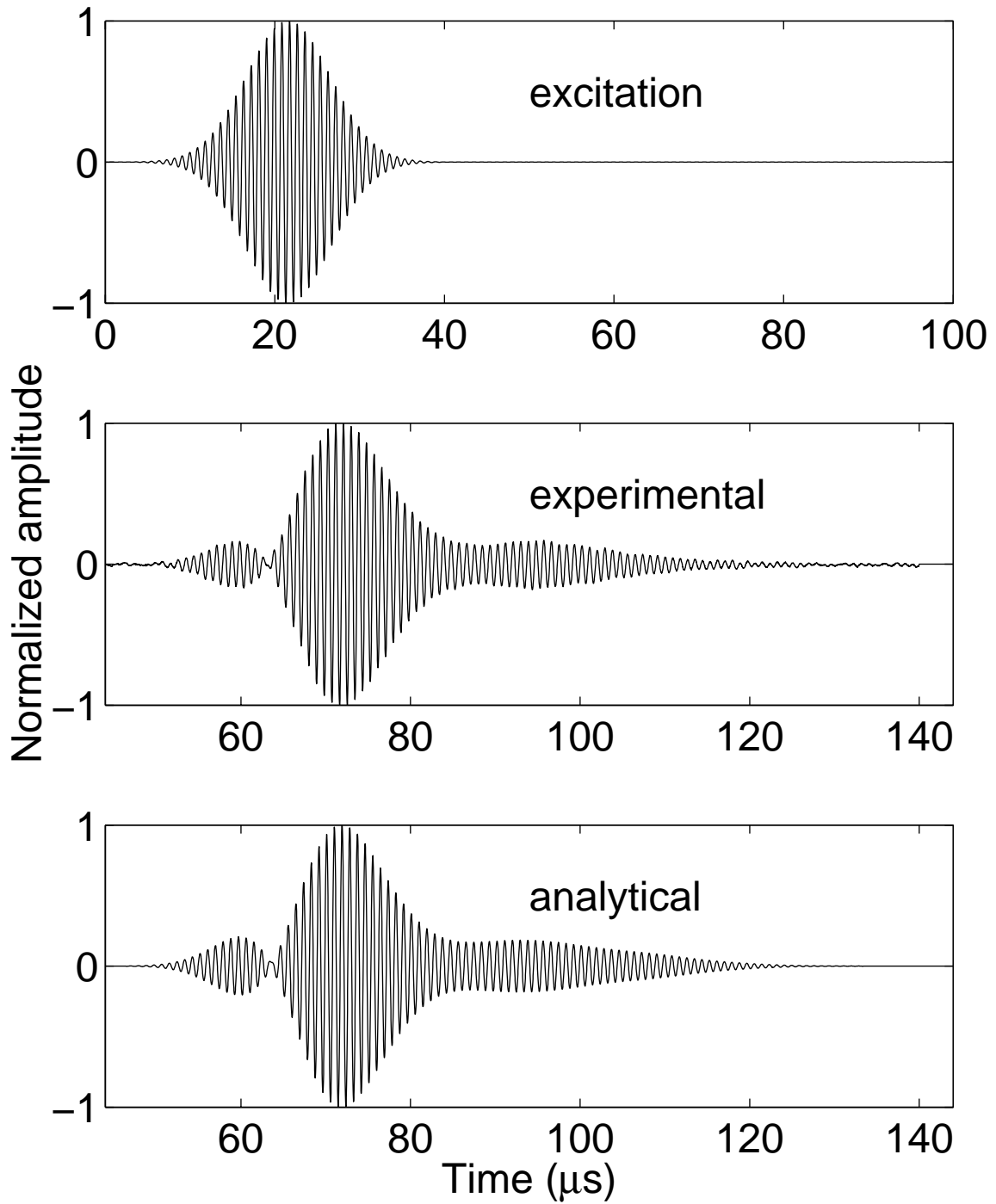


Fig. 6. 1107 kHz Gaussian excitation of a 0.25m long 25 mm diameter fused quartz waveguide. The excitation signal (top) is compared to the experimental received signal (middle) and the analytical signal (bottom).

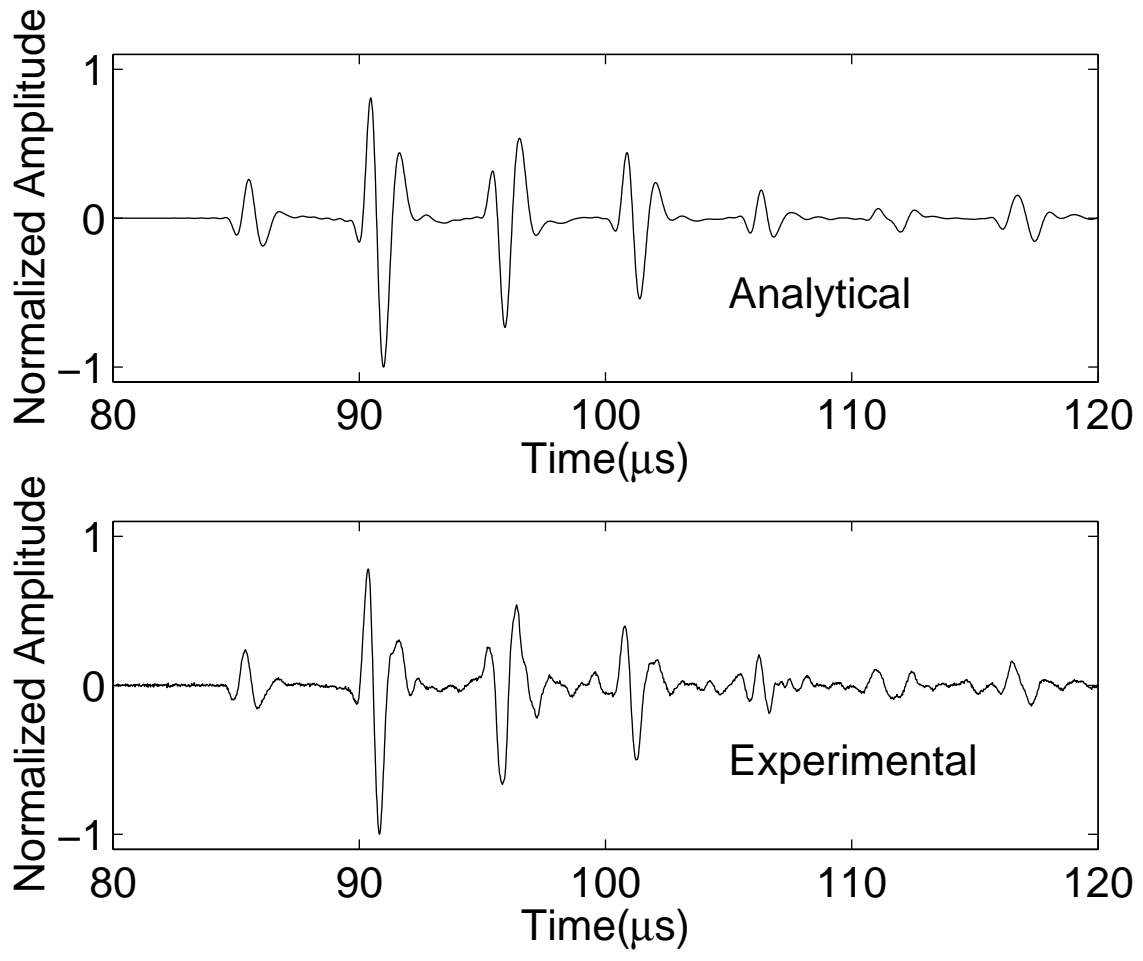


Fig. 7. Measured and calculated signals of a pulse propagated through a 0.5 m long 25 mm diameter fused quartz waveguide.

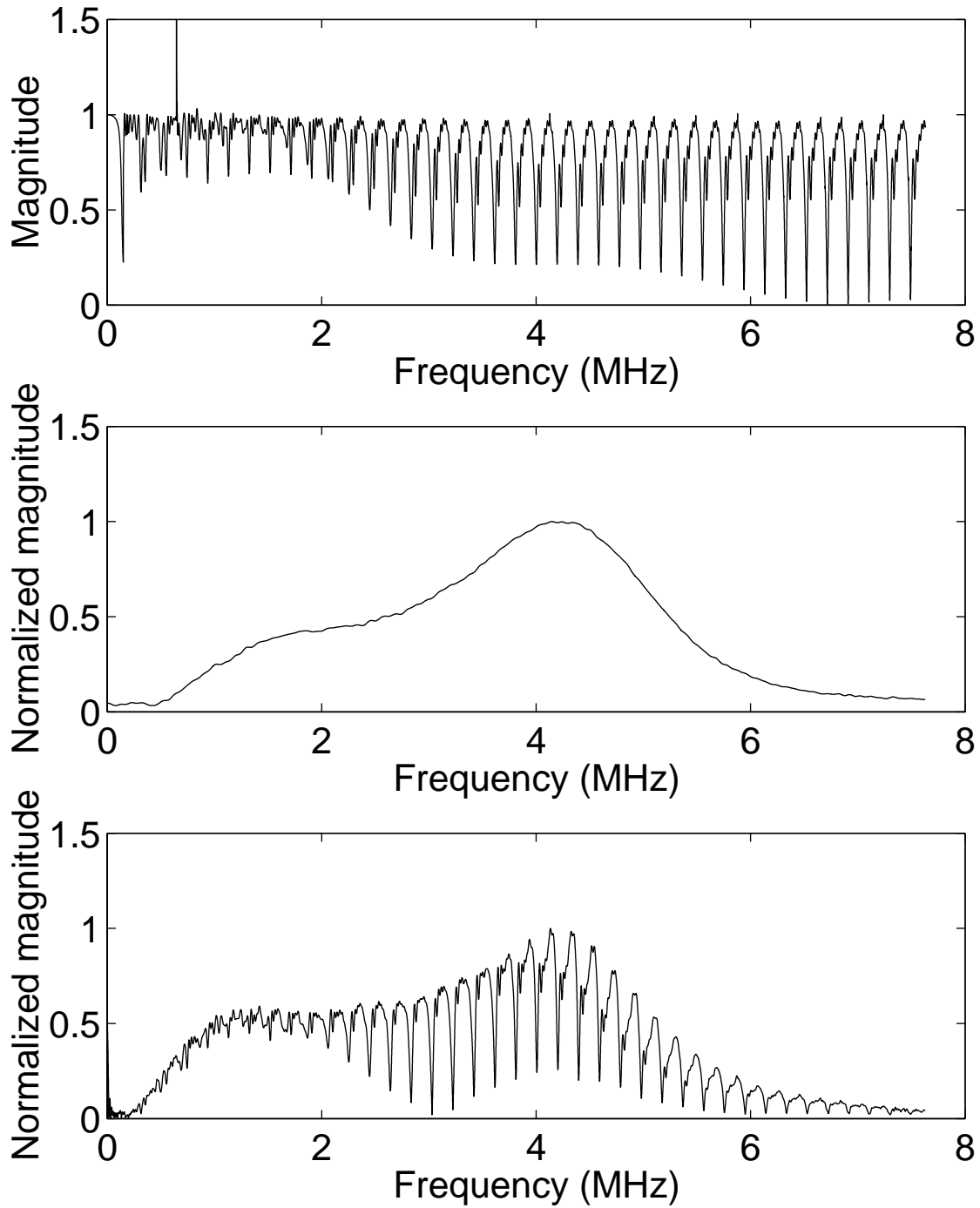


Fig. 8. The dispersion function for a 20 cm long, 25 mm diameter fused quartz waveguide (top), the magnitude of the frequency spectrum of an experimental signal before (middle) and after propagating through the waveguide (bottom).

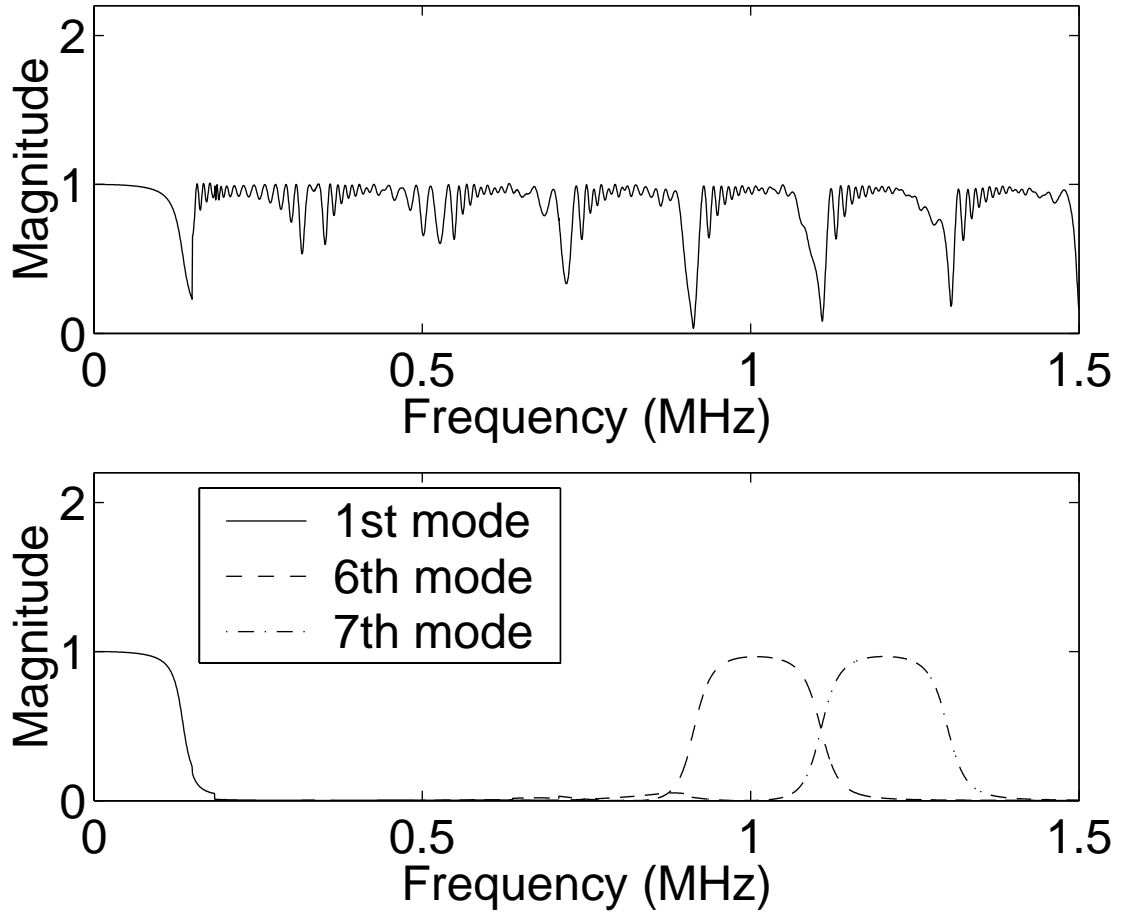


Fig. 9. Magnitude of the transfer function of the waveguide (top) and the magnitudes of the transfer functions of the 1st, 6th, and 7th modes (bottom). Transfer functions of the other modes are not shown for clarity.

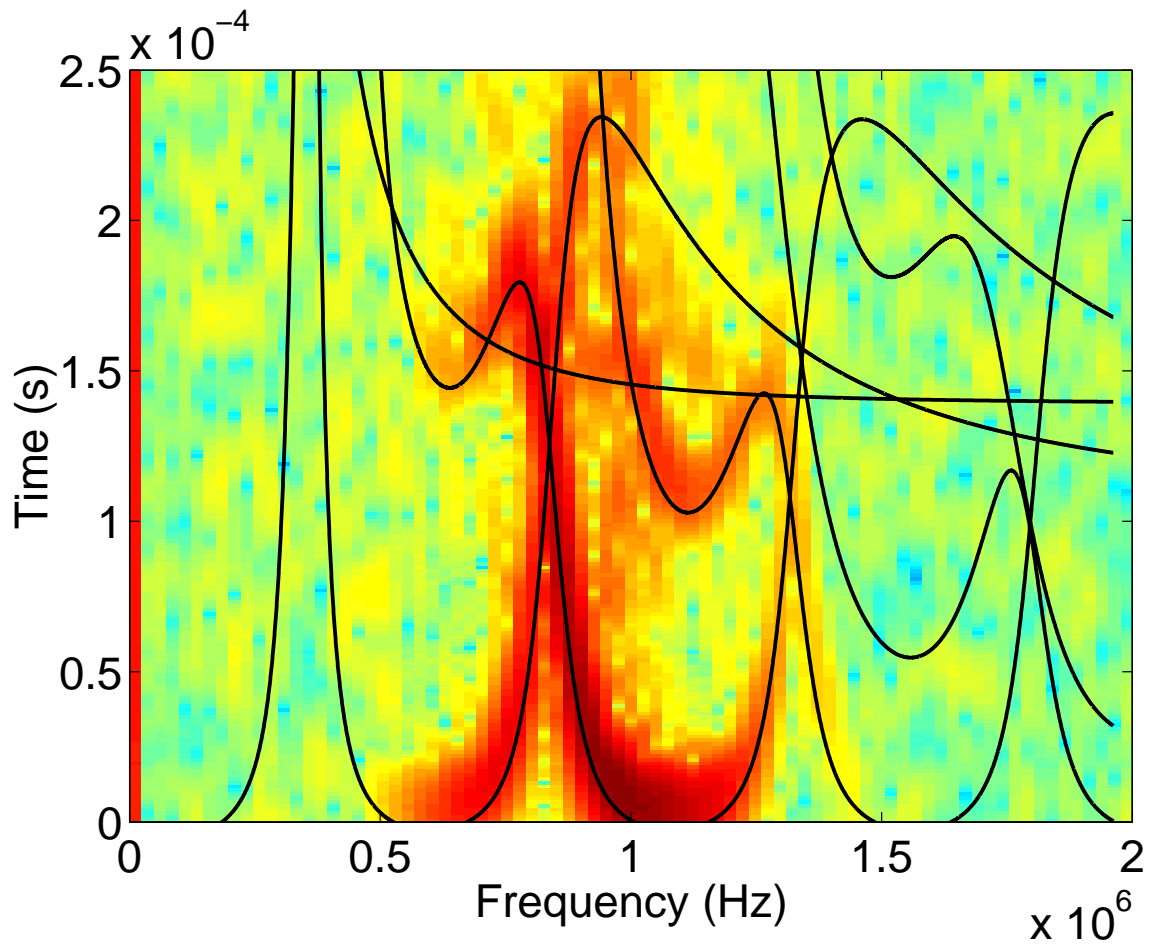


Fig. 10. Spectrogram of the experimental signal measured from a 1.22 m long 10 mm diameter fused quartz cylinder. Theoretical curves appear in black.

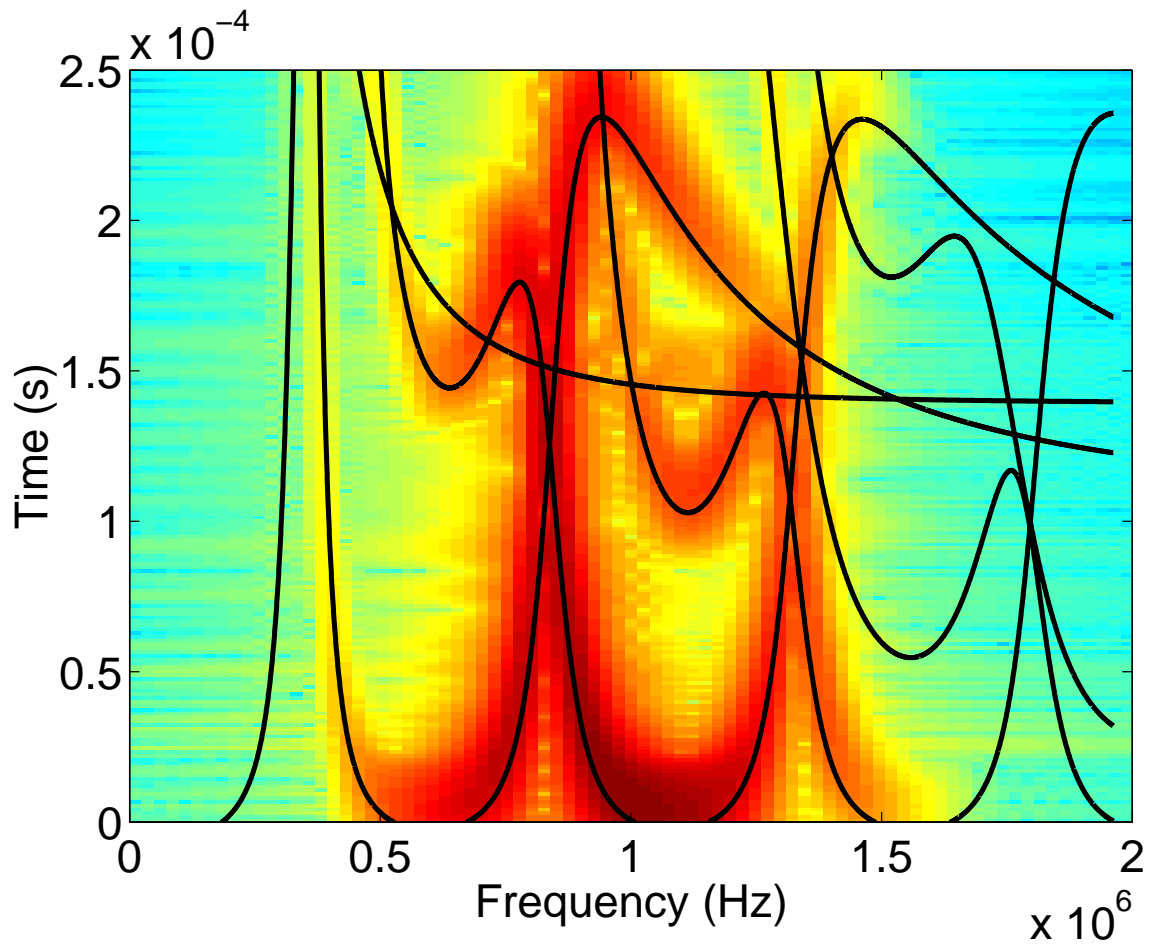


Fig. 11. Spectrogram of the analytical signal calculated for a 1.22 m long 10 mm diameter fused quartz cylinder. Theoretical curves appear in black.